Scientific paper

## Preparation of Porous Imidazole-based Poly(ionic liquid) Adsorbents and Their Toluene Adsorption Performance

Fangwen Luo, 1 Xujiao Tian, 1 Xian Dong, 1 Longchao Liang 1 and Zhuo Chen 1,\*

School of Chemistry and Material Science, Key Lab for Functional Material Chemistry, Guizhou Normal University, Guivang 550025, PR China

\* Corresponding author: E-mail: chenzhuo19@163.com

Received: 01-16-2024

#### **Abstract**

Efficient, economical, and durable adsorbents are required to remove volatile organic compounds (VOCs) from air. Cross-linked polyvinylic ionic liquids (PVIC) with porous structures were synthesized by quaternizing 1-vinylimidazole (1VI) with 1-bromobutane to obtain 3-butyl-1-vinylimidazolium bromide (VIC), which was then co-polymerized with divinylbenzene (DVB) radicals.  $^{1}$ H NMR,  $^{13}$ C NMR, scanning electron microscopy, X-ray photoelectron spectroscopy, Fourier-transform infrared spectroscopy, and N<sub>2</sub> adsorption–desorption isotherms were applied in characterizing the composites. Through modification of the polymer structure by adjustment of DVB concentration (the ratio of DVB concentration to VIC concentration was x: 1 (x = 0.4, 0.6, 0.8, 1.0) and the product was named PVIC-x (x = 2, 3, 4, 5)), the optimal PVIC-4 pore structure was obtained, with a specific surface area and total pore volume of 192.5 m² g⁻¹ and 0.192 cm³ g⁻¹, respectively. A toluene adsorption test verified the adsorption capacity. The adsorption behavior for VOCs, based on toluene, was investigated using adsorption breakthrough curves, adsorption kinetics, and isotherms. The adsorption process is well describing by the Bangham kinetic and Langmuir isotherm models. The dynamic adsorption of toluene was in the order of PVIC-4 > PVIC-5 > PVIC-3 > PVIC-2. The optimal toluene adsorption capacity of PVIC-4 was 264.4 mg g⁻¹ with an equilibrium time of 56 minutes, which was attributed to its excellent pore structure. PVIC-4 also performed well in terms of recycling rate, maintaining 91.19% adsorption efficiency after 5 cycles of recycling. PVIC-4 has the potential to remove volatile organic compounds from the air.

Keywords: Poly (ionic liquid)s; Imidazole; VOCs adsorption; Air purification

#### 1. Introduction

Volatile organic compounds (VOCs) are toxic airborne pollutants that deplete the ozone layer, contribute to global warming, and have major impacts on human health and the natural environment. Toluene is a VOC widely used as an organic solvent and a raw material in the synthesis of pharmaceuticals, explosives, and pesticides. It is also an essential component of many industrial and household products. Long-term exposure to toluene can cause severe damage to human respiratory, nervous, and hematopoietic systems. To a volume a volume to severe damage to human respiratory, nervous, and hematopoietic systems.

Previous studies have identified various methods for toluene removal from the atmosphere including adsorption,<sup>6,7</sup> thermal/catalytic oxidation,<sup>8,9</sup> photocatalytic degradation,<sup>10</sup> plasma-catalyzed processes ,<sup>11</sup> and biodegradation,<sup>12</sup> with adsorption being recognized as the optimal method due to its low cost, high efficiency, and simplicity. Adsorbent structure is the critical factor affecting adsorp-

tion capacity, directly influencing removal efficiency and operating cost. Various materials such as zeolites,<sup>13</sup> metal-organic materials,<sup>14</sup> bio-carbon materials,<sup>15</sup> carbon nanotubes,<sup>16</sup> and graphene,<sup>17</sup> have been applied as adsorbents, but their high cost, poor selectivity, low adsorption efficiency, and limited stability require improvement. The development of rapid and efficient adsorbents of high capacity is thus of practical importance in removing VOCs from the atmosphere.

Polyionic liquids (PILs) are polymeric materials synthesized by copolymeri-zation of ionic liquids (ILs) with another monomer. They combine the unique features of ILs and polymer structures with excellent performance in areas such as VOC adsorption, electrochemistry, and catalysis, <sup>18,19</sup> PILs have unique composite frameworks that maintain the superior properties of ILs combined with the stability, processability, durability, and controllability of polymeric materials, thereby overcoming many of the limitations of monomeric ILs.

Ionic liquids have received attention recently due to their excellent structural modifiability. Of 200 tested ILs, imidazolium-based ILs are ideal for toluene absorption, 20 and they have been used effectively for this purpose. 21,22 Use of poly-imidazolium ionic liquids (PVIMs) has been reported for the adsorption of dyes in water, 23 CO<sub>2</sub> in air, 24 and hemoglobin, 25 with a wide range of applications; however, efficient PVIM adsorption of toluene has yet to be reported. Frontier molecular orbital analysis indicates that the uptake of toluene by ILs is a physical process, 26 and their adsorption performance after polymerization depends mainly on pore volume, diameter, and shape, and specific surface area. Thus, the reproducible synthesis of porous poly imidazolium ILs (PVILs) as toluene adsorbents under mild conditions is challenging.

Here, PVIC-x of different structures were synthesized by quaternization and co-polymerization reactions involving 1-vinylimidazole (1VI), n-bromobutane, and divinylbenzene (DVB) with different DVB concentrations. The effect of crosslinker concentration on product pore structure was investigated, together with the reusability, adsorption breakthrough curves, kinetics, and isotherms characterizing the toluene adsorption behavior of PVIC-x. Their toluene adsorption mechanism was investigated through correlation of pore structure and adsorption capacity. The temperature of the adsorption process was 25°C to simulate an indoor environment, which is expected to play a role in removing toluene indoors.

### 2. Experimental

#### 2. 1. Materials

Chemicals used in this study were sourced in China as follows: 1-vinylimidazole, n-butyl bromide, divinylbenzene, and azodiisobutyronitrile from Aladdin Biochemical Technology, Shanghai; methanol, dichloromethane, anhydrous ethanol, and ethyl acetate from Fuyu Fine Chemical, Tianjin; toluene from Sinopharm Chemical Reagent, Shanghai; and anhydrous ether from Chuandong Chemical, Chongqing. All the chemicals were analytically pure and used without further purification. Water used in the experiments was deionized.

#### 2. 2. Synthesis of Imidazolium-based ILs

The IL precursor 3-n-butyl-1-vinylimidazolium bromide (VIC) was synthesized using published methods,<sup>27</sup>

as described in Scheme 1. Typically, 1-vinylimidazole (20 mmol) and n-butyl bromide (20 mmol) were mixed in a 100 mL flask with vigorous stirring under a nitrogen atmosphere. The mixture was refluxed at 70 °C for 24 h. After the reaction, the liquid phase was decanted off and the solid residue washed three times with ethyl acetate and ether, and dried at 50 °C for 12 h under vacuum. Found: 1H NMR (400 MHz, DMSO)  $\delta$  9.76 (s, 1H), 8.29 (s, 1H), 8.01 (s, 1H), 7.35 (d, 1H), 6.01 (d, 1H), 5.41 (d, 1H), 4.23 (t, 2H), 1.80 (m, 2H), 1.27 (d, 2H), 0.88 (t, 3H). 13C NMR (101 MHz, DMSO)  $\delta$  135.77, 129.32, 123.73, 119.65, 109.11, 49.39, 31.53, 19.26, 13.77.)

### 2. 3. Synthesis of Porous Copolymer

The porous poly(ionic liquid) was prepared through the radical co-polymerization of VIC and DVB and DVB, <sup>28</sup> as shown in Scheme 1. First, 10 mmol VIC was mixed with DVB at VIC/DVB mass ratios of 5:2, 5:3, 5:4, and 5:5 in round-bottomed flasks; 5 mmol of initiator Azoindiisobutyronitrile (AIBN) was then added sequentially with 5 mL anhydrous ethanol, 25 mL ethyl acetate, and 5 mL water. The mixture was refluxed under nitrogen at 80 °C for 24 h on an oil bath. After reaction, the white solid residue was filtered off and washed three times with anhydrous ethanol and ultrapure water before drying under vacuum at 50 °C for 12 h to obtain poly(3-butyl-1-vinylimidazolium bromide) or 'PVIC-x', where x denotes the concentration of DVB in the VIC/DVB mass ratio.

#### 2. 4. Sample Characterization

<sup>1</sup>H NMR and <sup>13</sup>C-NMR spectra were obtained with an NMR spectrometer (Avance Neo 400M; Bruker, United States of America) in Deuterium with dimethyl sulfoxide using Tetramethylsilane as an internal reference. Fourier-transform infrared (FTIR) spectra were recorded with a Nicolet iS50 (Nicolet iS50; Thermo, United States of America) spectrometer in the 4000-400 cm<sup>-1</sup> region. X-ray photoelectron spectroscopy (Kalpha, Thermo, USA) is used to study the surface composition of materials. High-resolution field-emission scanning electron microscopy (FES-EM; Supra55 Sapphire, Zeiss, German; 10Kv) was used to study the geometric morphology of materials. A fully automated specific surface area and porosity analyzer (ASAP 2460, Micrometrics, United States of America) was used in nitrogen adsorption-desorption performance tests. The sample was outgassed in the degassing port of the appa-

Luo et al.: Preparation of Porous Imidazole-based Poly(ionic liquid) ...

ratus at 503 K for 3 h before testing. The Brunauer Emmett Teller (BET) specific surface area, pore volume, and average pore size (Barrett Joyner-Halenda method) were calculated by device software.

#### 2. 5. Dynamic Adsorption Measurements

Dynamic adsorption test of toluene using a GC2060 gas chromatograph from Shanghai Ruimin Instrument Co. The specific parameters of the gas chromatograph are as follows: column temperature 130 °C, inlet temperature 200 °C, hydrogen flame detector temperature 135 °C, carrier gas N2. Before adsorption measurements, the material was heated at 373 K for 3 h to remove any water molecules already adsorbed. Toluene steam was produced by blowing a stream of nitrogen gas into liquid toluene using N2 carrier gas at a flow rate of 200 mL min<sup>-1</sup>. Adsorption took place within a quartz tube of 6 mm internal diameter and 650 mm length. Quartz wool was used to prevent material being blown out. The toluene concentration was stable at 400 ppm. The adsorption temperature was 298 K, and 50 mg of absorbent was used in each test. An online gas chromatograph with a flame-ionization detector was used to monitor toluene concentrations at reactor inlet and outlet. The toluene breakthrough time was defined as the time required for the outlet concentration to reach 5% of the inlet concentration. The adsorption capacity of the adsorbent was calculated by integrating the area under the obtained penetration curve, as follows (Eq. (1)):<sup>29</sup>

$$q_t = \frac{1}{m} \int_0^t v(C_0 - C_t) dt \tag{1}$$

Where  $q_t$  (mg g<sup>-1</sup>) is the amount of toluene adsorbed per unit mass of adsorbent at a given time t; m (g) is the quantity of adsorbent; v (mL min<sup>-1</sup>) is the gas flow rate; and  $C_0$  and  $C_t$  (mg mL<sup>-1</sup>) are the initial inlet and outlet toluene concentrations at time t, respectively. After the adsorbent was saturated, the toluene gas flow was closed, and toluene desorbed at 100 °C at a nitrogen flow rate of 50 mL min<sup>-1</sup> until the concentration of toluene gas stream at the outlet was 0

#### 2. 6. Adsorption Theory and Models

Pseudo-first order (Eq. (2)),<sup>30</sup> pseudo-second order (Eq. (3)),<sup>31</sup> and Bangham (Eq. (4))<sup>32</sup> kinetics were used to describe the adsorption of toluene. The Weber-Morris pore diffusion model (Eq. (5)) <sup>33</sup> was used to further analyze the diffusion mechanism of toluene within the material.

$$q_{t} = q_{e} \left[ 1 - e^{-k_{I}t} \right] \tag{2}$$

$$q_t = \frac{k_2 q_e^2 t}{1 + k_2 q_e t} \tag{3}$$

$$q_t = q_e - \frac{q_e}{e^{kt^2}} \tag{4}$$

$$q_{\cdot} = k_{\cdot} t^{1/2} + C_{\cdot}$$
 (5)

where  $q_e$  (mg g<sup>-1</sup>) is the amount of toluene adsorbed at adsorption equilibrium; t (min) is the adsorption time;  $k_1$  (min<sup>-1</sup>),  $k_2$  (g mg<sup>-1</sup> min<sup>-1</sup>), and k (min<sup>-1</sup>) are rate constants for the proposed first-order, second-order, and Bangham kinetic equations, respectively;  $k_i$  (mg (g·min<sup>1/2</sup>)) and  $C_i$  (mg g<sup>-1</sup>) are the intra-particle diffusion coefficient and intercept, respectively; and z is a constant

The adsorption process of toluene by each material was elucidated by the fitting of isotherms using the Langmuir (Eq. (6)),(Eq. (7))<sup>34</sup> and Freundlich (Eq. (8))<sup>35</sup> models

$$q_e = \frac{q_m K_L C}{I + K_L C} \tag{6}$$

$$R_L = \frac{1}{1 + K_r C} \tag{7}$$

$$q_e = K_F C^{1/n} \tag{8}$$

where  $q_e$  and  $q_m$  (mg g<sup>-1</sup>) are the equilibrium and maximum adsorption volumes, respectively; C (mg m<sup>-3</sup>) is the equilibrium concentration;  $K_L$  (L mg<sup>-1</sup>) and  $K_F$  ((mg g<sup>-1</sup>)/ (mg L<sup>-1</sup>)<sup>1/n</sup>) are constants of the Langmuir and Freundlich models,  $R_L$  stands for Langmuir dimensionless separation factor, respectively; and n is Freundlich heterogeneity factor.

#### 3. Results and Discussion

#### 3. 1. Characteristics of PVIC-x

Copolymer material polymerized from DVB and VIC, the copolymer mate-rials were further characterized by FTIR spectroscopy. The spectra of synthesized PVIC-x are shown in Fig. 1 for characteristic vibrations in the pol-

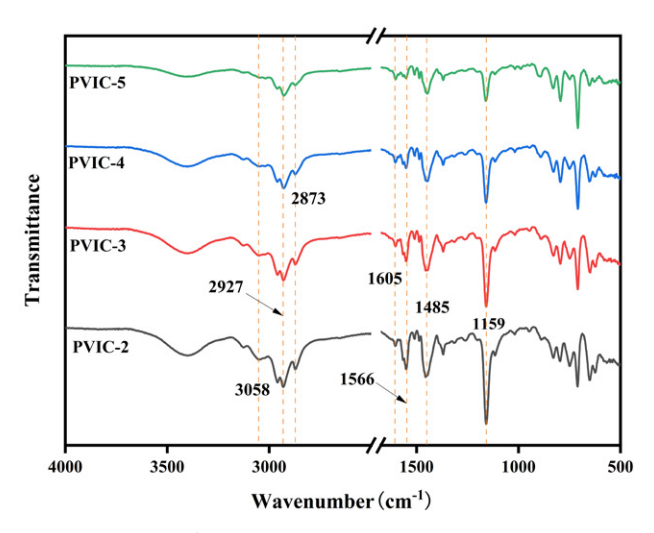


**Figure 1.** FT-IR of PVIC-x

ymers regarding DVB correlation: bands at 3058 and 3016 cm<sup>-1</sup> represent aromatic C–H stretching vibrations, and the band at 2927 cm<sup>-1</sup> represents aliphatic C–H stretching vibrations. Bands at 1485 and 1446 cm<sup>-1</sup> represent aromatic C–H in-plane and bending vibrations, respectively.<sup>36,37</sup> For the imidazole-IL portion of the polymer, the aliphatic C–H turning vibration band is at 2873 cm<sup>-1</sup>, and the imidazole ring backbone band at 1566 cm<sup>-1</sup>. The imidazole ring in-plane C–H bond bending vibration is at 1159 cm<sup>-1</sup>.<sup>38</sup> As the synthesized polymers differed only in the ratio of reactants, there was little variation in IR spectra of the corresponding copolymers. These results indicate that both imidazole-IL and DVB precursors were retained in the copolymers, and the polymers were successfully synthesized.

The chemical states of the elements in PVIC-x were investigated using X-ray photoelectron spectroscopy (XPS). Taking PVIC-4 as an example, the investigated XPS spectra (Fig. 2a) clearly show the presence of C 1s, N 1s, and Br 3d. The high-resolution spectra of these

elements are shown in Fig. 2b-d. For example, the C 1s spectrum has three peaks at 284.8, 285.9, and 285.8 eV attributed to carbon atoms in the carbon chain, C-N, and benzene ring, respectively. In the N 1s spectrum, peaks at 400.4 eV and 398.3 eV can be assigned to N-C and N=C in imidazole indicating successful incorporation of imidazole moiety. In the Br 3d spectrum, the peaks at 70.0 eV and 68.9 eV are from the Br  $3d_{5/2}$  spin brbital and Br  $3d_{3/2}$ , respectively.

The surface morphologies of the fabricated polymeric adsorbents (PVIC-2, PVIC-3, PVIC-4, and PVIC-5) were studied by FESEM (Fig. 3). For a ratio of cross-linker DVB of 2/5 (PVIC-2), the prepared polymer had a 'lumpy' structure with a rough surface, cracks, and irregular particles on the surface (Fig. 3a). As the DVB ratio increased, unstable particles on the surface became smaller, and pore structures became evident with a trend towards a spherical shape (Fig. 3b), increasing to a large number of spherical and globular like combinations of the

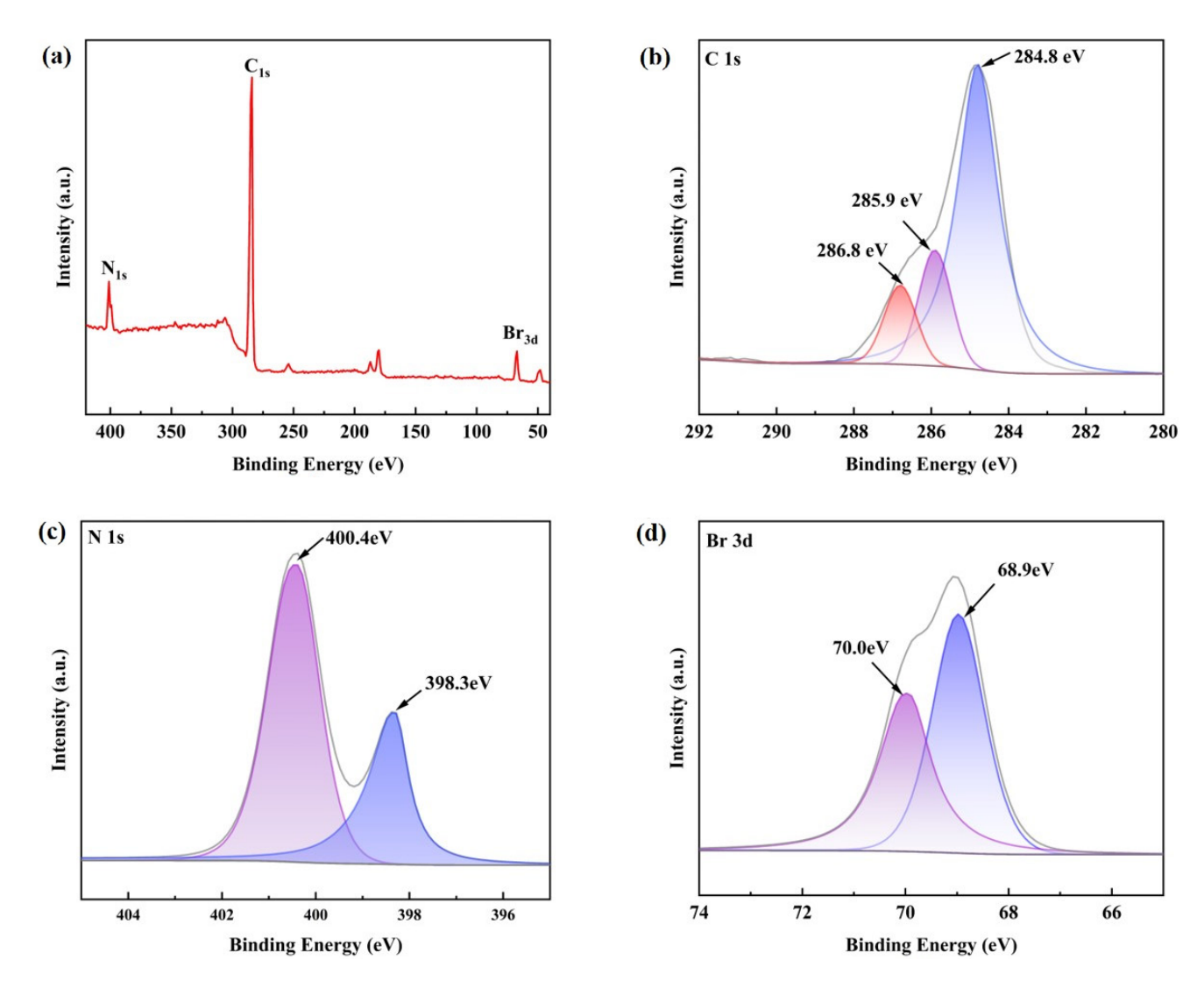


Figure. 2. XPS spectra of PVIC-4: (a) survey spectra, (b) C 1 s, (c) N 1 s, (d) Br 3 d

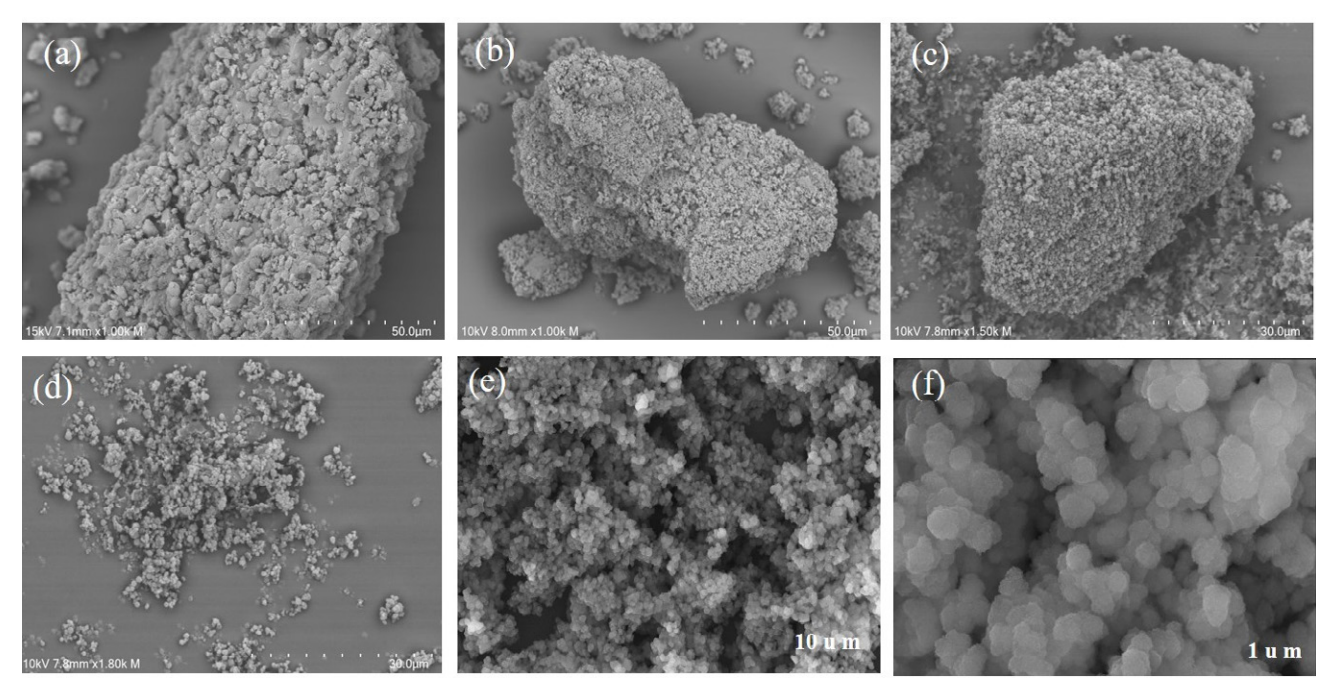


Figure 3. SEM images: (a) PVIC-2; (b) PVIC-3; (c) PVIC-4; (d) PVIC-5; (e) PVIC-4; (f) PVIC-4

clusters (Fig. 3c). Finally, the globular cluster structure collapsed to form a dispersed disordered state (Fig. 3d). The disordered pore structure is a typical feature of adsorbent materials, providing both transport channels and adsorption sites for adsorbate molecules. PVIC-4 had a porous structure (Fig. 3e–f), with macropores providing the main diffusion channels for adsorbate molecules to enter the interior of the adsorbent, with adsorption increasing with the proportion of cross-linker DVB. However, when the DVB ratio reached the same proportion as that of VIC, the cluster structure collapsed, resulting in a dense and disordered surface (PVIC-5) with a reduced pore structure.

The structure characteristics of PVIC-2, PVIC-3, PVIC-4, and PVIC-5 adsorbents were characterized by BET technology. The results are shown in Figure 4, and the pore structure parameters are shown in Table 1.

Based on the International Union of Pure and Applied Chemistry adsorption isotherm classification, the prepared PVIC-2, PVIC-3, PVIC-4, and PVIC-5 absorbents had type IV isotherms with  $H_4$ -type hysteresis loops (Fig. 4a). The hysteresis loops closed at a relative pressure of  $P/P_0 = 0.4$ , due to capillary condensation of  $N_2$  molecules in the mesoporous structure, thereby indicating the presence of smaller mesopores. At low relative pressure ( $P/P_0 < 0.01$ ), the material exhibited some adsorption of  $N_2$ ,

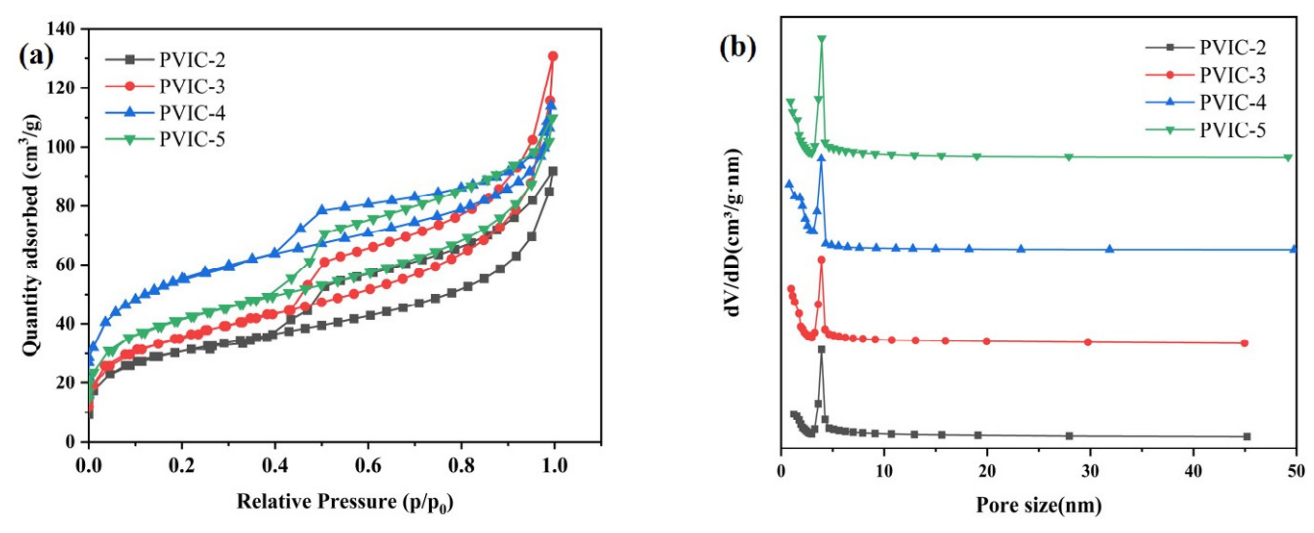


Figure 4. (a) N<sub>2</sub> adsorption-desorption isotherms (b) N<sub>2</sub> adsorption-desorption isotherm: log scale and the pore size distribution curves

Table 1. Physical parameters of PVIC-x

Adsorbents	Surface (m <sup>2</sup> /g)				Pore volume (cm <sup>3</sup> /g)			D <sub>p</sub> (nm)
	$S_{BET}$	$S_{mic}$	S <sub>mes</sub>	$S_{mic}/S_{BET}$	$V_{tot}$	$V_{mic}$	$V_{mic}/V_{tot}$	•
PVIC-2	109.8	17.9	91.9	16.3%	0.142	0.0131	9.20%	5.83
PVIC-3	128.3	27.1	101.2	21.1%	0.151	0.0198	13.10%	7.11
PVIC-4	192.5	41.8	150.7	21.7%	0.192	0.0323	16.80%	4.36
PVIC-5	152.4	35.9	116.5	23.5%	0.169	0.0241	14.30%	5.28

 $S_{BET}$ : total specific surface area;  $S_{mic}$ : microporous surface area;  $S_{mes}$ : mesoporous surface area;  $V_{tot}$ : total pore volume;  $V_{mic}$ : microporous pore; Dp: average pore size

likely due to the strong interaction between the microporous structure and  $N_2$  molecules increasing the adsorption capacity of  $N_2$ , and indicating the presence of micropores.<sup>42</sup>

The pore-size distribution curves (Fig. 4b) indicate bimodal distributions for PVIC-3, PVIC-4, and PVIC-5, with peaks at 1 and 4 nm. This further indicates that the adsorbents had typical micro mesoporous structures.<sup>43</sup> All

adsorbents were porous, predominantly with mesopores and some micropores (Table 1). The specific surface area and total pore volume of the adsorbents tended to increase then decrease with increasing cross-linker concentration. This was likely due to an increase in the number of DVB molecules and changes of reaction sites within VIC during cross-linking, which promoted the formation of the pore structure. PVIC thus has an effective pore structure

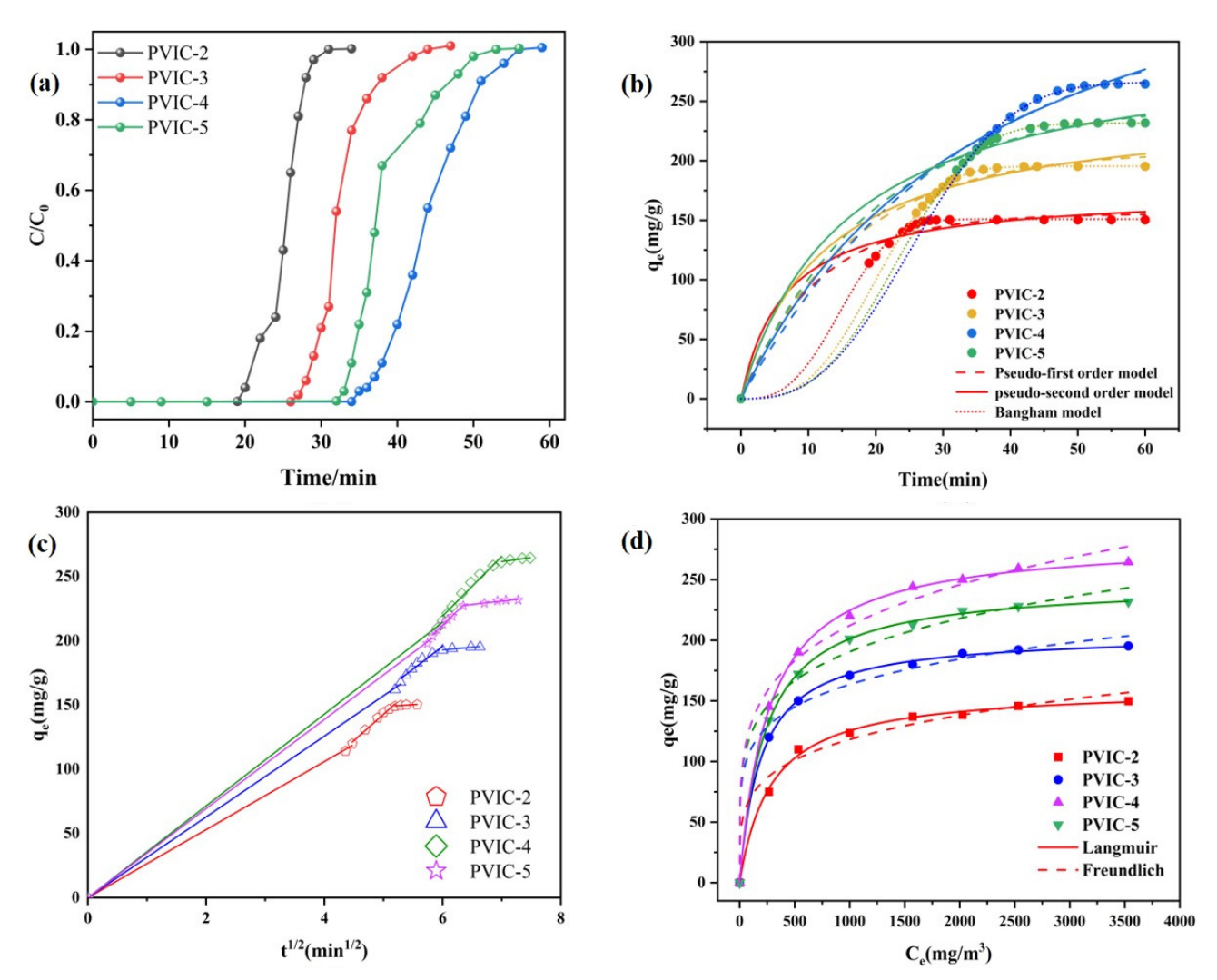


Figure 5. (a) Adsorption breakthrough curves of toluene on PVIC-x. (b) pseudo-first order, pseudo-second order models and Bangham model, (c) intra-particle diffusion model, (d) Langmuir and Freundlich models

at PVIC-4, with a specific surface area of 192.5  $\rm m^2\,g^{-1}$ , total pore volume of 0.192  $\rm cm^3\,g^{-1}$ , and microporous ratio of 16.8%. As the DVB concentration continued to increase towards PVIC-5, the specific surface area of the adsorbent decreased to 152.4  $\rm m^2\,g^{-1}$  and the pore volume to 0.169  $\rm cm^3\,g^{-1}$ . This may be due to excess DVB molecules filling the pore volume. Finally, the adsorbent could not maintain the clustering, and it collapsed.

# 3. 2. Dynamic Adsorption Performance of Toluene

The prepared PVIC-2, PVIC-3, PVIC-4, and PVIC-5 PIL adsorbents were used for the adsorptive removal of toluene, with results shown in Fig. 4a. The toluene breakthrough time, adsorption equilibrium time, and equilibrium adsorption capacity of the PILs are provided in Table S1

The adsorption process of all adsorbents could be divided into three stages (Fig. 5a) as follows. (1) During the initial stage of pre-adsorption, the adsorption curve is nearly level at zero, and the adsorbent adsorbs all the surface toluene molecules with a zero-export concentration. (2) During the middle stage, the adsorbent is penetrated by toluene molecules. As adsorption proceeds, the export concentration gradually increases, as indicated by the rising adsorption curve (Fig. 5a). (3) During the late stage, an increasing number of toluene molecules penetrate the adsorbent, with increasing export concentration. When the toluene concentrations in the inlet and outlet are approximately equal, the adsorption has reached dynamic equilibrium. 44 Toluene adsorption followed the order PVIC-4 > PVIC-5 > PVIC-3 > PVIC-2 (Table S1). Changes in DVB concentration affected the adsorbent pore structure, and adsorption by PVIC-4 was highest due to its optimal BET and total pore volume, consistent with its structural properties.

The toluene adsorption mechanism of the prepared PVIC-x was investigated by nonlinear fitting of the adsorption curves using the proposed first-order, second-order, and Bangham kinetic models (Fig. 5b). The relevant parameters for the three model fittings are given in Table S2

For the three dynamic models, there was little difference between the theoretical adsorption obtained by fitting of the Bangham equation and experimentally observed adsorption (Fig. 5b; Table S2). determination coefficients ( $R^2$ ) were all >0.999, indicating that the Bangham kinetic model is most suitable for describing the adsorption of toluene by PVIC-x, this is consistent with the presence of both mesopores and micropores in its structure. The Bangham model is generally used to describe orifice diffusion processes. Adsorption by all PVIC adsorbents involves mainly surface and pore diffusion. Surface diffusion occurs mainly in the adsorption stage, when toluene molecules occupy adsorption sites on the adsorbent surface, with high adsorption efficiency.<sup>45</sup> As the adsorption

process continues, the increasing number of toluene molecules on the surface reduces the number of adsorption sites available, causing some toluene molecules to diffuse into the interior of the pore structure to occupy internal adsorption sites. The pore structure of PVIC-x thus has a major influence on the adsorption process. The proposed first-order kinetic model describes the physical adsorption process, while the quasi-second-order model is more suitable for describing the chemical adsorption process. The fitting of the former was significantly better than that of the latter, indicating that physical interaction is the main control of the adsorption rate of toluene.<sup>46</sup>

The fitting curves and parameters of the intra-particle diffusion model are provided in Fig. 5c and Table S3, which indicate that the physical adsorption of toluene by PVIC-x can be also divided into three stages<sup>47</sup> as follows. (1) During the external diffusion stage, the main influencing factor is the specific surface area; the larger the area, the higher the diffusion coefficient  $k_1$ . (2) During the internal diffusion stage,  $C_2$  is non-zero and, in addition to diffusion resistance inside the particles, the adsorption process may be subject to other influencing factors. (3) During the adsorption equilibrium stage, a comparison of the diffusion coefficients (k) of the three stages indicated that  $k_2 > k_1 > k_3$ . The adsorption rate was thus highest in stage (2), with internal diffusion playing an essential role.

The experimental data were also fitted according to the Langmuir and Freundlich models (Fig. 5d; Tables S4), with the correlation coefficient of the former being nearer 1 than that of the latter, implying that toluene adsorption involves monolayer adsorption. The difficulty of adsorption was assessed by calculating the dimensionless separation factor,  $R_L(\text{If }R_L=0\text{ means that the process is irreversible, }0 < R_L < 1\text{ means that the adsorption is favorable, }R_L=1\text{ means that the adsorption process is unfavorable), with all RL values being between 0 and 1, implying that toluene has a strong affinity for each material. The <math>n$  values (heterogeneity factors) in the Freundlich model were used to identify adsorption processes; 1/n was < 1, implying that toluene adsorption involved a physical process.

# 3. 3. Relationship Between Pore Structure and Adsorption Capacity

To understand the effect of pore structure on the material's performance in the adsorption of toluene, a linear correlation analysis was performed between the adsorption capacity and the specification of the material's micropores and mesoporous.

The effect of pore structure on toluene adsorption performance was investigated by correlation analysis between adsorption capacity and characteristics of material micro- and mesopores. Adsorption capacity was strongly correlated with surface area and micropore volume ( $R^2 = 0.9966$  and 0.9636, respectively; Fig. 6a, c) compared with

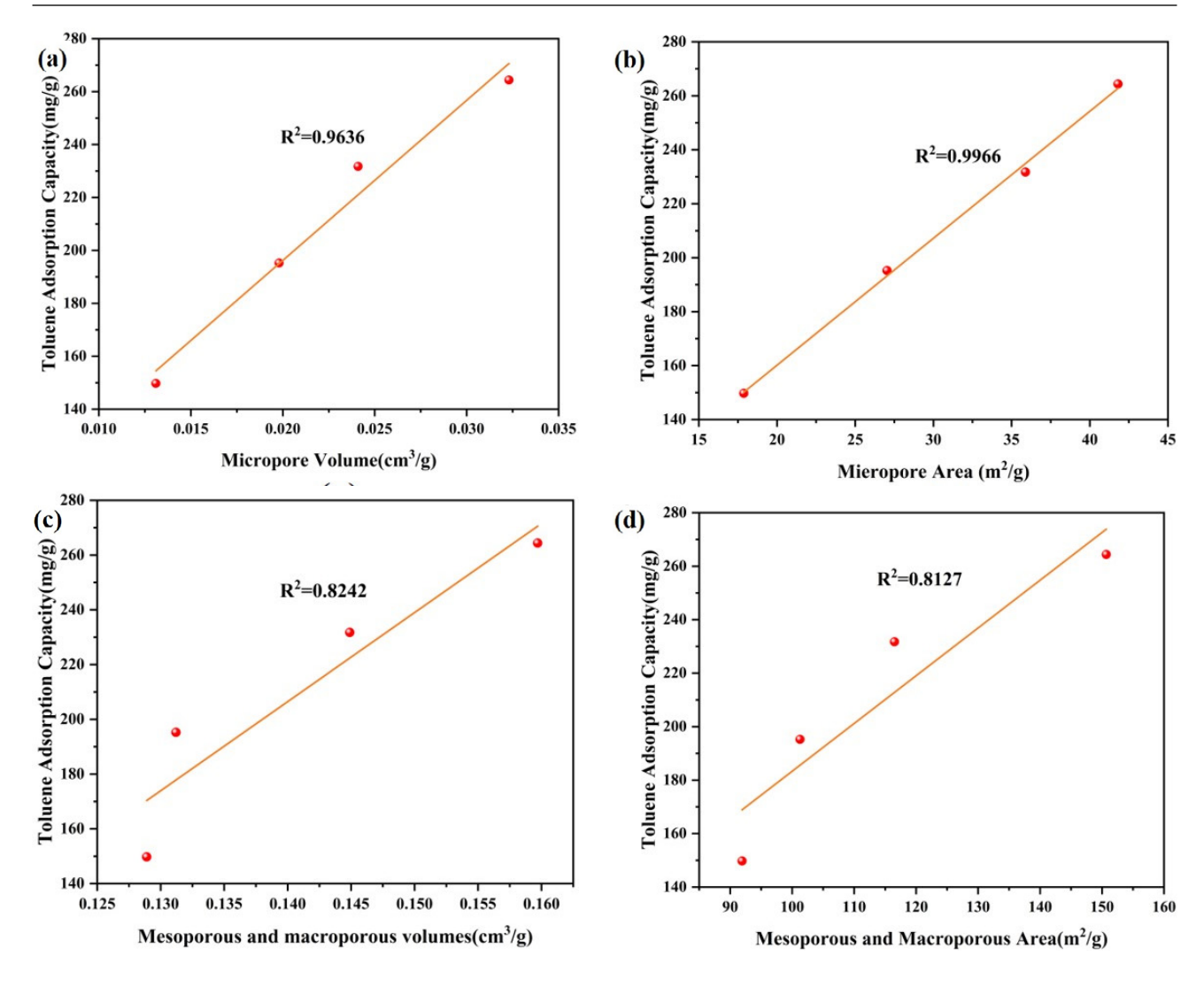


Figure 6. The relationship between toluene adsorption capacity and (a) microporous volume, (b) micropore area, (c) mesopores and macropore volume, and (d) mesopore and macropore area.

surface area or mesopore volume ( $R^2 = 0.8127$  and 0.8242, respectively; Fig. 6b, d). The adsorption capacity of PVIC for toluene is thus affected mainly by the microporous structure of the material itself. The weaker contribution of meso- and macro-pores to toluene adsorption is likely due to their acting mainly as transport channels during adsorption, rather than acting as adsorption sites.<sup>51</sup> It follows that the microporous structure is the main site of toluene adsorption by PVIC-x.

Table 2 systematically lists the comparison between the materials synthesized in this study and the commonly used toluene trapping adsorbents in the literature. The results show that the adsorption of toluene by the PVIC-4 material is improved compared to zeolite and organic polymers, but it has some shortcomings compared to IL/MOF composites and there is room for further optimization, which can be achieved by modulating the anionic and cationic structure of the ionic liquids.<sup>56</sup>

**Table 2**. Comparison of toluene capture performances with other adsorbents from literature.

Material	Toluene sorption capacity	Ref
Triphenylamine-based conjugated organic polymers	s 78mg/g	Lan et al <sup>52</sup> .,2021
S-S spherical zeolite	93mg/g	Chen et al53.,2022
[BMIM][CH <sub>3</sub> COO]/UiO-66 (1% wt.)	197mg/g	Ramos et al <sup>54</sup> .,2022
[BMIM][CH3COO]/MIL101 (10% wt.)	680mg/g	Ramos et al55.,2023
PVIC-4	264mg/g	This work

In terms of adsorption mechanism, the adsorption of toluene by PVIC-x is mainly physical adsorption. The process can be divided into three stages, the first is the outer surface diffusion stage, where toluene is transferred to the outer surface of the adsorbent. Secondly, there is an internal diffusion stage, in which toluene diffuses through the pores into the inner surface, and the pore structure and volume are the dominant factors. Finally, there is the adsorption equilibrium stage, in which the adsorption sites are fully occupied and the adsorption slowly reaches equilibrium. In addition to physical adsorption, there is also some chemical adsorption, which is mainly attributed to  $\pi$ - $\pi$  stacking interactions between toluene molecules and aromatic molecules of PIL, hydrogen bonding, and electrostatic interactions.

#### 3. 4. Reusable Properties of Adsorbents

Adsorbent reusability is vital for practical commercial applications. As PVIC-4 had the optimal adsorption performance, it was selected for reproducibility performance study.

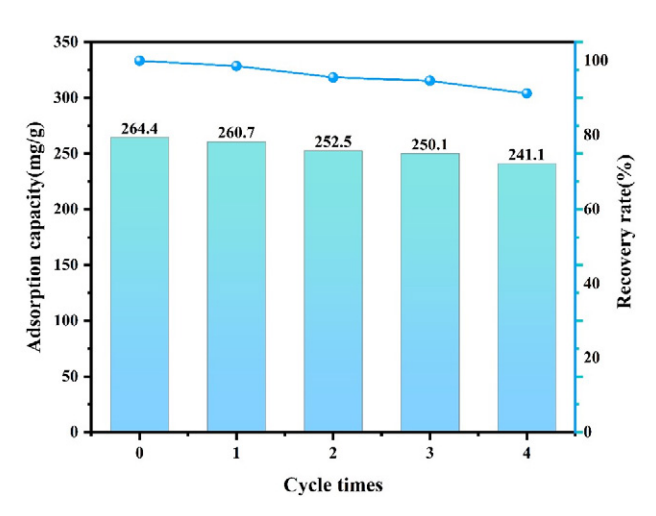


Figure 7. The reusability performance of PVIC-4.

The cyclic adsorption experiments of the adsorbent were carried out in the dynamic adsorption experimental setup. The desorption temperature of the adsorbent was increased from 25 °C to 130 °C at a rate of 10 °C/min, and the desorption gas flow was a 20 ml/min nitrogen flow, and the temperature was maintained at 130 °C until no toluene was detected at the gas chromatography detection outlet.

In five adsorption–desorption cycling experiments with new PVIC-4 material, the adsorption efficiency was 98.60%, 95.50%, 94.59%, and 91.19% (from the second cycle) (Fig. 7). The decrease in adsorption capacity may be due to pore blockage and coalescence, which would hinder the desorption of adsorbed toluene.<sup>57</sup>

However, PVIC-4 still maintained >90% adsorption after several cycles, demonstrating satisfactory reusability.

#### 4. Conclusions

PVIC adsorbents with different pore structures were synthesized using imidazolium-based ILs as raw materials and DVB as a cross-linking agent. FTIR spectroscopy confirmed that monomer copolymerization with DVB was successful. With specific microporous structures, BET-specific surface areas of PVIC-x tended to increase and then decrease with an increasing proportion of cross-linking agents. Breakthrough curves indicate that surface area and pore volume improve toluene adsorption capacity. Bangham kinetics and Langmuir isotherms adequately described the toluene adsorption behavior of PVIC-4 material, with its adsorption mechanism involving mainly physical interaction where toluene is adsorbed on the surface before diffusion within pore space. Together with a model of intra-particle distribution, this suggests that the intraparticle diffusion stage is the primary rate-limiting step for toluene adsorption by PVIC-x. The adsorption capacity of PVIC-4 remained above 90% after five use cycles, with robust toluene adsorption and regeneration performance. Analysis of the relationship between pore structure and adsorption capacity indicated that the microporous structure had a major influence on PVIC toluene adsorption capacity. Our findings indicate that PVIC-x are a promising adsorption material, indicating the need for future studies of VOC adsorption by PILs.

#### **Supporting Information**

Supporting information sheets S1, S2, S3 and S4 are available from the Annex.

#### 5. References

- X. Li, L. Zhang, Z. Yang, P. Wang, Y. Yan and J. Ran, Sep. Purif. Technol, 2020, 235. DOI:10.1016/j.seppur.2019.116213
- C. Liu, W. Cai and L. Liu, Appl. Clay Sci, 2018, 162, 113–120.
   DOI:10.1016/j.clay.2018.06.005
- 3. M. Tang, X. Huang, Y. Peng and S. Lu, *Fuel*, **2020**, 270. **DOI:**10.1016/j.fuel.2020.117478
- 4. L. Lan, Y. Huang, Y. Dan and L. Jiang, *React. Funct. Polym*, **2021**, *159*. **DOI:**10.1016/j.reactfunctpolym.2020.104804
- A. A. Rico-Barragán, J. R. Álvarez, S. Pioquinto-García, J. Rodríguez-Hernández, P. Rivas-García and N. E. Dávila-Guzmán, Sustain. Prod. Consump, 2023, 40, 159–168.
   DOI:10.1016/j.spc.2023.06.011
- J. Yang, M. Gao, S. Wang, M. Zhang, L. Chen, J. Su, Y. Huang,
   Y. Zhang, X. Wang and B. Shen, ACS Appl. Mater. Interfaces,
   2022, 14, 40052–40061. DOI:10.1021/acsami.2c11700

- X. Pan, N. Zhang, L. Yang, C. He, X. Ma, X. Liu, L. Liu, T. Hou and Y. Jiao, ACS Omega, 2023, 8, 39329-39344.
   DOI:10.1021/acsomega.3c04866
- 8. J. Shao, F. Lin, Z. Wang, P. Liu, H. Tang, Y. He and K. Cen, *Appl. Catal.*, *B*, **2020**, *266*. **DOI**:10.1016/j.apcatb.2020.118662
- S. Mo, Q. Zhang, J. Li, Y. Sun, Q. Ren, S. Zou, Q. Zhang, J. Lu, M. Fu, D. Mo, J. Wu, H. Huang and D. Ye, *Appl. Catal.*, *B*, 2020, 264. DOI:10.1016/j.apcatb.2019.118464
- J. Zhang, Y. Hu, J. Qin, Z. Yang and M. Fu, Chem. Eng. J, 2020, 385. DOI:10.1016/j.cej.2019.123814
- B. Zhu, L.-Y. Zhang, M. Li, Y. Yan, X.-M. Zhang and Y.-M. Zhu, Chem. Eng. J, 2020, 381. DOI:10.1016/j.cej.2019.122599
- R. Ghasemi, F. Golbabaei, S. Rezaei, M. R. Pourmand, R. Nabizadeh, M. J. Jafari and E. Masoorian, *AMB Express*, 2020, 10, 8. DOI:10.1186/s13568-019-0941-z
- M. Kraus, U. Trommler, F. Holzer, F.-D. Kopinke and U. Roland, *Chem. Eng. J*, **2018**, *351*, 356–363.
   DOI:10.1016/j.cej.2018.06.128
- 14. K. Vellingiri, P. Kumar, A. Deep and K.-H. Kim, *Chem. Eng. J*, **2017**, *307*, 1116-1126. **DOI:**10.1016/j.cej.2016.09.012
- 15. E. David, *Materials (Basel)*, **2022**, *16* (1). **DOI:**10.3390/ma16010389
- A. E. Memetova, I. V. Burakova, A. E. Burakov, N. R. Memetov and A. G. Tkachev, *Adsorpt.-J. Int. Adsorpt. Soc*, 2023, 29, 335–349. DOI:10.1007/s10450-023-00405-y
- L. Wang and L. Hong, J. Spat. Sci, 2019, 66, 75–87.
   DOI:10.1080/14498596.2019.1601137
- M. H. Jing, X. M. Song, D. W. Fang, L. Zhang and Q. Zhang, *Talanta*, **2019**, *197*, 277–283.
   DOI:10.1016/j.talanta.2018.12.101
- 19. D.-J. Tao, F. Liu, L. Wang and L. Jiang, *Appl. Catal.*, *A: General*, **2018**, 564, 56-63. **DOI**:10.1016/j.apcata.2018.07.018
- J. Bedia, E. Ruiz, J. de Riva, V. R. Ferro, J. Palomar and J. J. Rodriguez, *AICHE J*, **2012**, *59*, 1648–1656.
   **DOI:**10.1002/aic.13926
- 21. X. Yan, S. Anguille, M. Bendahan and P. Moulin, *Chem. Eng. J.* **2021**, 404. **DOI:**10.1016/j.cej.2020.127109
- X. Ma, W. Wang, C. Sun and J. Sun, *Environ Pollut*, **2021**, 285, 117675. **DOI**:10.1016/j.envpol.2021.117675
- J. Lin, T. Su, J. Chen, T. Xue, S. Yang, P. Guo, H. Lin, H. Wang,
   Y. Hong, Y. Su, L. Peng and J. Li, *Chemosphere*, 2021, 272,
   129640. DOI:10.1016/j.chemosphere.2021.129640
- L. Sun, M. Gao and S. Tang, *Chem. Eng. J*, **2021**, *412*.
   DOI:10.1016/j.cej.2021.128764
- X.-F. Wang, Y. Zhang, Y. Shu, X.-W. Chen and J.-H. Wang, RSC Adv, 2015, 5, 31496–31501. DOI:10.1039/C5RA00036J
- L. Tan, J. Zhu, M. Zhou, X. He and S. Zhang, *J. Mol. Liq*, 2020,
   DOI:10.1016/j.molliq.2019.112054
- 27.M. Xin, J. Qiang, L. Zi, and K. Yuan, *J. Am. Chem. Soc.* **2005**, 127 (27), 9694–9695. **DOI**:10.1021/ja051803v
- 28. P. Zhao, Y. Leng and J. Wang, *Chem. Eng. J* **2012**, 204–206, 72-78. **DOI:**10.1016/j.cej.2012.07.097
- B. Lei, H. Xie, S. Chen, B. Liu and G. Zhou, *Environ Sci Pollut Res Int*, 2020, 27, 27072–27092.
   DOI:10.1007/s11356-020-09115-2
- 30. M. Li, Y. Li, W. Li, F. Liu, X. Qi, M. Xue, Y. Wang and C. Zhao,

- *Environ Sci Pollut Res Int*, **2020**, *27*, 6052-6065. **DOI:**10.1007/s11356-019-07293-2
- X. Yang, H. Yi, X. Tang, S. Zhao, Z. Yang, Y. Ma, T. Feng and X. Cui, *J Environ Sci (China)*, 2018, 67, 104–114.
   DOI:10.1016/j.jes.2017.06.032
- B. Lei, B. Liu, H. Zhang, L. Yan, H. Xie and G. Zhou, *J Environ Sci (China)*, 2020, 88, 122–132.
   DOI:10.1016/j.jes.2019.07.001
- 33. T. B. Nuria Fiol, *J. Chem. Eng. Process Technol*, **2013**, *04* (06). **DOI**:10.4172/2157-7048.1000165
- 34. G. Zhang, Y. Liu, S. Zheng and Z. Hashisho, *J Hazard Mater*, **2019**, *364*, 317–324. **DOI:**10.1016/j.jhazmat.2018.10.031
- 35. M. Mozaffari Majd, V. Kordzadeh-Kermani, V. Ghalandari, A. Askari and M. Sillanpaa, *Sci Total Environ*, **2022**, *812*, 151334. **DOI:**10.1016/j.scitotenv.2021.151334
- 36. X. Huang, Y. Wang, Y. Liu and D. Yuan, *J Sep Sci*, **2013**, *36*, 3210–3219. **DOI:**10.1002/jssc.201300355
- A. Pourjavadi, S. H. Hosseini and Z. S. Emami, *Chem. Eng. J*,
   2013, 232, 453–457. DOI:10.1016/j.cej.2013.07.090
- 38. X. Feng, C. Gao, Z. Guo, Y. Zhou and J. Wang, *RSC Adv.*, **2014**, *4*, 23389–23395. **DOI**:10.1039/C4RA03163F
- X. Tian, F. Luo, X. Dong, L. Liang, Y. Duan, J. Zhuang and Z. Chen, *Colloids Surf.*, A, 2024, 682.
   DOI:10.1016/j.colsurfa.2023.132883
- J. Olvera-Mancilla, C. Aguilar-Lugo, L. Fomina, F. M. Sanchez-Arevalo, M. O. González-Díaz, R. Sulub-Sulub, M. Aguilar-Vega and L. Alexandrova, *Ind. Eng. Chem. Res.*, 2022, 61, 6587–6599. DOI:10.1021/acs.iecr.2c00020
- 41. Y. Wang, W. Chen, B. Zhao, H. Wang, L. Qin and J. Han, *RSC Adv*, **2020**, *10*, 23749–23758. **DOI:**10.1039/D0RA02225J
- W. Sun, J. Li, H. Li, B. Jin, Z. Li, T. Zhang and X. Zhu, Chemosphere, 2022, 296, 133962.
   DOI:10.1016/j.chemosphere.2022.133962
- 43. G. Zhang, B. Lei, S. Chen, H. Xie and G. Zhou, *J. Environ. Chem. Eng*, **2021**, 9. **DOI:**10.1016/j.jece.2021.105387
- 44. Y. Chen, C. Fan, X. Li, J. Ren, G. Zhang, H. Xie, B. Liu and G. Zhou, J. Chem. Technol. Biotechnol, 2022, 98, 117–128.
  DOI:10.1002/jctb.7220
- 45. L. Largitte, T. Brudey, T. Tant, P. C. Dumesnil and P. Lodewyckx, *Microporous Mesoporous Mat*, **2016**, *219*, 265–275. **DOI:**10.1016/j.micromeso.2015.07.005
- 46. M. Ş. Ece, S. Kutluay, Ö. Şahin and S. Horoz, *Ind. Eng. Chem. Res*, **2020**, 59, 21106–21123. **DOI**:10.1021/acs.iecr.0c03883
- 47. X. Zhang, X. Miao, W. Xiang, J. Zhang, C. Cao, H. Wang, X. Hu and B. Gao, *J Hazard Mater*, **2021**, *403*, 123540. **DOI:**10.1016/j.jhazmat.2020.123540
- 48. T. K. Das, Q. Scott and A. N. Bezbaruah, *Chemosphere*, **2021**, 281, 130837. **DOI:**10.1016/j.chemosphere.2021.130837
- 49. W. Zou, B. Gao, Y. S. Ok and L. Dong, *Chemosphere*, **2019**, 218, 845-859. **DOI**:10.1016/j.chemosphere.2018.11.175
- O. Sahin, S. Kutluay, S. Horoz and M. S. Ece, *Environ Sci Pollut Res Int*, 2021, 28, 5231–5253.
   DOI:10.1007/s11356-020-10885-y
- Y. N. Prajapati, B. Bhaduri, H. C. Joshi, A. Srivastava and N. Verma, *Chemosphere*, **2016**, *155*, 62–69.
   **DOI:**10.1016/j.chemosphere.2016.04.040

- D. Chen, Q. Tang and W. Deng, *Microporous Mesoporous Mat.*,
   2022, 346:112275. DOI:10.1016/j.micromeso.2022.112275
- L Lan, Y Huang and Dan Y, React. Funct. Polym, 2021, 159:104804. DOI:10.1016/j.reactfunctpolym.2020.104804
- Ventura C. R., H. Wei and Yeung K. L., *Environ Res*, 2022, 215(Pt 3): 114341. DOI:10.1016/j.envres.2022.114341
- Ventura C. R., H. Wei and Zhang X, Environ Res, 2023, 219: 115000. DOI:10.1016/j.envres.2022.115000
- Ventura C. R., H. Wei and Yeung K. L., Green Chem. Eng.,
   2020, 1(2): 147–154. DOI:10.1016/j.gce.2020.10.008
- Z. An, S. Kong, W. Zhang, M. Yuan, Z. An and D. Chen, *Materials (Basel)*, 2020, 13. DOI:10.3390/ma13030716

#### Povzetek

Za odstranjevanje hlapnih organskih spojin (VOCs) iz zraka so potrebni učinkoviti, ekonomični in trajni adsorbenti. Zamrežene polivinilne ionske tekočine (PVIC) s porozno strukturo so bile sintetizirane s kvaternizacijo 1-vinilimidazola (1VI) z 1-bromobutanom, da smo dobili 3-butil-1-vinilimidazolijev bromid (VIC), ki je bil nato kopolimeriziran z radikali divinilbenzena (DVB). Za karakterizacijo kompozitov smo uporabili <sup>1</sup>H NMR, <sup>13</sup>C NMR, vrstično elektronsko mikroskopijo, rentgensko fotoelektronsko spektroskopijo, infrardečo spektroskopijo s Fourierjevo transformacijo in N<sub>2</sub> izoterme adsorpcije-desorpcije. S spremembo strukture polimera s prilagoditvijo koncentracije DVB (razmerje med koncentracijo DVB in koncentracijo VIC je bilo x: 1 (x = 0,4,0,6,0,8,1,0) in product je bil poimenovan PVIC-x (x = 2,3,4,5)), je bila pridobljena optimalna struktura por PVIC-4 s specifično površino in skupnim volumnom por 192,5 m² g⁻¹ oziroma 0,192 cm³ g⁻¹. Preskus adsorpcije toluena je potrdil adsorpcijsko kapaciteto. Adsorpcijsko obnašanje za VOCs na osnovi toluena je bilo raziskano z adsorpcijskimi prebojnimi krivuljami, adsorpcijsko kinetiko in izotermami. Adsorpcijski proces dobro opisujeta Banghamov kinetični in Langmuirjev izotermni model. Dinamična adsorpcija toluena je bila v vrstnem redu PVIC-4 > PVIC-5 > PVIC-3 > PVIC-2. Optimalna adsorpcijska kapaciteta toluena PVIC-4 se je dobro odrezal tudi glede stopnje recikliranja, saj je po 5 ciklih recikliranja ohranil 91,19-odstotno učinkovitost adsorpcije. PVIC-4 lahko odstrani hlapne organske spojine iz zraka.



Except when otherwise noted, articles in this journal are published under the terms and conditions of the Creative Commons Attribution 4.0 International License